Cancer Letters 461 (2019) 65–77

Contents lists available at ScienceDirect

Cancer Letters

journal homepage: www.elsevier.com/locate/canlet

Original Articles

Identification of a CIP4 PKA phosphorylation site involved in the regulation of cancer cell invasiveness and metastasis

Facundo M. Tonucci[a], Evangelina Almada[a], Carla Borini-Etichetti[a], Alejandro Pariani[a], Florencia Hidalgo[a], M. Jose Rico[b], Javier Girardini[c], Cristián Favre[a], James R. Goldenring[d], Mauricio Menacho-Marquez[e], M. Cecilia Larocca[a,*]

[a] Instituto de Fisiología Experimental, Facultad de Ciencias Bioquímicas y Farmacéuticas, Universidad Nacional de Rosario (UNR), Consejo de Investigaciones Científicas y Técnicas (CONICET), Rosario, Argentina
[b] Instituto de Genética Experimental, Facultad de Ciencias Médicas - UNR, Rosario, Argentina
[c] Instituto de Inmunología Clínica y Experimental de Rosario, Argentina
[d] Epithelial Biology Center and Department of Cell & Developmental Biology, Vanderbilt University School of Medicine, Nashville, TN, USA
[e] Instituto de Investigaciones para el Descubrimiento de Fármacos-Laboratorio Max Plank de Rosario, UNR - CONICET, Rosario, Argentina

ARTICLE INFO

Keywords:
AKAP350
AKAP450
CDC42
Invadopodia
Cell-migration

ABSTRACT

CDC42 interacting protein 4 (CIP4) is a CDC42 effector that coordinates membrane deformation and actin polymerization. The correlation of CIP4 overexpression with metastatic capacity has been characterized in several types of cancer. However, little information exists on how CIP4 function is regulated. CIP4 interacts with A-kinase (PKA) anchoring protein 350 (AKAP350) and CIP4 is also a PKA substrate. Here, we identified CIP4 T225 as the major CIP4 PKA phosphorylation site. *In vitro* and *in vivo* experiments using hepatocellular carcinoma (HCC) and breast cancer cells showed that expression of a CIP4(T225E) phosphomimetic mutant increased cancer cell metastatic capacity and that, conversely, expression of a CIP4(T225A) non-phosphorylatable mutant reduced invasive properties. PKA inhibition decreased to CIP4(T225A) cell-levels control but not CIP4(T225E) cell migratory and invasive efficiency. Concomitantly, our studies indicate that CIP4 T225 phosphorylation promotes the formation of functional invadopodia and enhances CIP4 localization at these structures. Our findings further provide mechanistic data indicating that CIP4 T225 phosphorylation facilitates CIP4 interaction with CDC42. Altogether this study identifies a signaling pathway that involves CIP4 phosphorylation by PKA during the acquisition of a metastatic phenotype in cancer cells.

1. Introduction

CIP4 (TRIP10) is an adaptor protein initially identified by its interaction with the activated form of CDC42 [1]. Structurally, CIP4 belongs to the family of F-BAR proteins. These F-BAR proteins contain an amino-terminal Fes-CIP4 homology domain followed by a coiled-coil region (F-BAR or extended FER CIP4 homology (EFC) domain), which interacts with negatively charged membrane phospholipids promoting membrane curvature [2]. CIP4 also contains a Src Homology 3 (SH3) domain at the carboxyl terminus that mediates its interaction with the proline-rich domains of WASP and its related proteins WAVE and N-WASP, which are activators of the Arp2/3 complex and promote local formation of branched actin filaments [3,4]. By means of its SH3 domain, CIP4 also interacts with formins Dia and DAAM1, which generate nucleation of linear actin filaments, and with dynamin-2 [3,5,6]. Hence, CIP4 coordinates membrane deformation with vesicle scission and actin polymerization, participating in processes that involve generation of membrane protrusions, endocytosis and vesicle movement [4].

Other studies have demonstrated that CIP4 overexpression correlates with cell invasiveness and metastatic capacity in osteosarcoma, breast cancer, non-small lung and nasopharyngeal cancer cells [7–12]. Our own investigations have shown that CIP4 participates in the acquisition of migratory properties in HCC cells [13]. The pro-metastatic role of CIP4 has been particularly well characterized in breast cancer. In MDA-MB-231 triple negative breast cancer cells, CIP4 is fundamental

Abbreviations: AKAP350, A-kinase anchoring protein 350; CIP4, CDC42 interacting protein 4; CIP4 WT, CIP4 wild type; FRET, Imaging Förster resonance energy transfer; HCC, hepatocellular carcinoma; PKA, protein kinase A; SH3, Src Homology 3

* Corresponding author. Suipacha 531, 2000, Rosario, Argentina.
E-mail address: larocca@ifise-conicet.gov.ar (M.C. Larocca).

https://doi.org/10.1016/j.canlet.2019.07.006
Received 4 January 2019; Received in revised form 8 July 2019; Accepted 11 July 2019

for invadopodia formation and, therefore, for cell invasiveness in response to EGFR activation [7]. Furthermore, Rolland and colleagues demonstrated that, in normal breast epithelial cells, CIP4 promotes E-cadherin endocytosis and disruption of cellular junctions, which are the initial events in the acquisition of a migratory phenotype [8]. That study also showed that CIP4 levels are significantly increased in clinically aggressive breast cancers and that, even in breast tumors that usually have good prognosis, CIP4 overexpression is associated with disease relapse. Similar results were obtained by an independent study, which also identified CIP4 as a potential biomarker for poor prognosis in human breast cancer patients [11].

Even though most of the evidence collected in normal epithelia and cancer cells positions CIP4 as a prometastatic protein, studies performed in fibroblast-derived cells and in breast cancer cells that overexpress Src kinase showed that CIP4 can negatively regulate cell migration and invadopodia function [14,15]. Those results suggest that the pro-invasive effects of CIP4 are cellular context-dependent. CIP4 interacts with the A-kinase anchoring protein AKAP350 (also known as AKAP450 or AKAP9) by means of its F-BAR domain [16]. In this scenario, AKAP350, which itself regulates metastatic features in several cancer cells [13,17–19], represents a likely candidate to regulate CIP4 function. In fact, our recent studies indicate that, in HCC cells, CIP4 interaction with AKAP350 is important for the acquisition of the migratory phenotype that enables directional cell migration [13]. CIP4 is an endogenous PKA substrate [16]. The role for PKA in tumor cell acquisition of invasive properties is complex, since it is dependent on the substrates that PKA phosphorylates in each specific condition [20]. In the present study, we evaluated the effect of CIP4 phosphorylation by PKA on the modulation of the invasive properties of HCC and breast cancer cells and characterized the mechanisms involved in this activity.

2. Materials and methods

2.1. Cell culture

MDCK cells were obtained from Keith Mostov lab (UCSF, CA). HepG2/C3a and MDA-MB-231 cells were purchased from the American Type Culture Collection. Cells were grown on plastic flasks in Dulbecco's modified Eagle's medium with 4.5 gm of glucose/L, supplemented with 10% fetal bovine serum and antibiotics. Cells were tested monthly by PCR for contamination with mycoplasma.

2.2. Relevance of AKAP350 expression on CIP4 phosphorylation in situ

Cells with decreased AKAP350 expression were prepared using a lentiviral system to express two different AKAP350 specific short hairpin RNAs (shRNA1 and shRNA4) as described [13]. Silencing was confirmed by western blotting and immunofluorescence analyses, using mouse monoclonal anti-AKAP350 (14G2) antibody [13,21]. CIP4 immunoprecipitation and identification of its phosphorylation in RXXS/T residues was performed using Phospho-PKA substrate antibody (Cell Signalling), as described in the supplementary material.

2.3. Identification of CIP4 PKA phosphorylation site

In silico identification of putative PKA substrate sites in CIP4 sequence was performed using three phosphorylation sites prediction servers: Expassy bioinformatics portal (http://www.cbs.dtu.dk/services/NetPhosK/) [22], Group-based phosphorylation scoring method (http://www.phospho.elm.eu.org) and Prediction of PK-specific Phosphorylation site (http://www.ppsp.biocuckoo.org) [23]. Mutants of the putative phosphorylation sites were prepared using a Quickchange method with complementary mutated primer sequences and a full length CIP4 cDNA cloned into the pET30c vector [15] as template to amplify CIP4 sequence by PCR. The recombinant proteins were produced using BL21(DE3)pLysS bacteria and purified using Ni-beads and CIP4 *in vitro* phosphorylation was assessed as described in Supplementary methods.

2.4. Generation of CIP4 wild type (CIP4 WT), CIP4(T225A) and CIP4(T225E) cell lines

Plasmids for expression of CIP4T225 mutants in HepG2 cells were generated by using Quickchange complementary mutated primers and pEGFP-CIP4 plasmid [13] as template to amplify CIP4 sequence by PCR. The pEGFP plasmids containing CIP4 WT, CIP4(T225A) or CIP4(T225E) sequences were used as templates to clone each of the CIP4 sequences into the retroviral vector pLPC (Clontech), which were used to generate MDA-MB-231 CIP4 WT, CIP4(T225A) or CIP4(T225E) cells. Detailed information about those procedures and cell transfection and selection are available in the Supplementary methods section.

2.5. Evaluation of CIP4 T225 phosphorylation at cellular level

MDA-MB-231 CIP4WT and CIP4T225A cells were incubated with 10 μM Forskolin (Sigma) for 10 min. After incubation, cells were scraped into cold PBS containing protease and phosphatase inhibitors (Sigma-Aldrich). Cells were lysed and immunoprecipitates were prepared by using mouse anti-GFP antibody (abcam, #ab290) and analyzed by Western blot by using an antibody that recognizes the phosphorylated RXXS/T site or anti-GFP as described in the Supplementary methods section.

2.6. Wound healing and in vitro invasion assays

HepG2 or MDA-MB-231 cells seeded at 2.5×10^6 cells in 2 ml of DMEM were cultured overnight at 37 °C in 6-well plates. Cell cultures were wounded by dragging a 100 μl pipette tip through the monolayer, washed using PBS to remove cellular debris and allowed to migrate. For MDA-MB-231 experiments, images of wounds in the same field were captured when the wound was introduced (0 h) and 6 h after wounding using an inverted microscope. Wound closure was assessed using ImageJ software. For HepG2 experiments, cells were fixed at 6 h or 24 h after the wound was performed, immunostained and analyzed by confocal microscopy as described in the Supplementary methods. The front-rear migratory polarity was evaluated at 6 h by measuring the distance from the nucleus, the centrosome or the cell centroid to the wound edge, and calculating the distance from the nucleus and the centrosome to the cell centroid, as we have previously described [13]. *In vitro* cell invasion assays were performed in 10 mm diameter and 8 μm pore polycarbonate filter Transwell plates. Membranes were precoated with 20 μg of matrigel, which formed a reconstituted basement membrane at 37 °C. Suspensions of 1×10^5 HepG2 or 5×10^4 MDA-MB-231 cells in serum-free DMEM were added to the upper chamber, and the lower chamber was filled with medium containing 10% fetal bovine serum. After 48 h for HepG2 cells or 24 h for MDA-MB-231 cells, cells that had invaded the lower chamber were fixed with methanol, stained with 1% Toluidine Blue in 1% borax for 5 min, and counted using an inverted microscope.

2.7. Animal studies

Experiments were performed using 6 week-old female athymic nude mice (6 per group), obtained from the School of Veterinary Sciences at the National University of La Plata. During the experiments, the animals were treated in accordance with the Canadian Council on Animal Care guidelines. To analyze the effect of CIP4 T225 mutants on the ability of HCC cells to invade and colonize the lungs, HepG2 cells were suspended in PBS (2×10^7 cells per ml). One hundred μl of the suspension was injected into the mouse lateral tail vein (experimental metastasis studies). In order to analyze the effect of CIP4 T225 mutants on the tumorigenic and metastatic properties of breast cancer cells, MDA-MB-

231 cells were suspended (2×10^7 cell per ml) in an ice-cold 50:50 solution of Matrigel and PBS. Fifty µl of the final cell suspension was introduced into the right inguinal mammary gland of anaesthetized mice using a 25-gauge needle. Primary tumor growth was analyzed by measuring tumor length (a) and width (b) with a caliper every 3-4 days, and tumor volume (V) was calculated using the formula $V = 0.4\,ab^2$. After 8 weeks in experimental metastasis, or 12 weeks in spontaneous metastasis experiments, mice were euthanized, the chest cavity was exposed through a midline chest incision, the trachea cannulated with a 20-gauge needle and lungs slowly inflated using 1 ml of India ink (1:16 in PBS). Lungs were extracted, immersed in Fekete's solution and metastatic nodules were counted visually. Lungs were embedded in paraffin and cut into 4 µm sections and stained with hematoxylin and eosin. Additionally, lung sections were analyzed by immunohistochemistry using an anti-pan-cytokeratin antibody (Santa Cruz-8018, C-11, 1:50) developed with a Vectastain ABC Kit (Vector laboratories).

2.8. Invadopodia formation and gelatin degradation assays

We evaluated the formation of functional invadopodia as previously described [24]. Briefly, cells were plated on coverslips coated with gelatin conjugated to FITC (Thermo Fisher Scientific: G13187) in 6-well plates at 4 x10^4 cells/ml, incubated 16 h at 37 °C and then fixed and stained with phalloidin-Alexa 555 and rabbit anti-cortactin-antibody (GTX100253). Images were obtained using a Nikon C2+ confocal system mounted on a Nikon TiE inverted microscope. Foci of degraded matrix were visible as dark areas of 0.2–1.2 µm in diameter in the bright fluorescent gelatin matrix. A cell generating at least one “hole” under the cell or near the cell edge was counted as a cell able to degrade extracellular matrix (ECM). Functional invadopodia were identified as actin- and cortactin-rich membrane structures localized close to sites of degraded ECM. To assess localization of CIP4 mutants at invadopodia, cells were grown on Matrigel–coated dishes at 4 x10^4/ml in complete medium, allowed to invade for 16 h, and invadopodia were identified as previously described [14]. Invadopodia were counted from 6 to 10 random fields in each sample and averaged over three independent experiments.

2.9. Imaging förster resonance energy transfer (FRET) measurements

In the present study, the acceptor bleaching FRET method was used, as previously described in detail [25] using an LSM880 confocal with an ObserverZ1 inverted microscope. GFP-CIP4 chimeric proteins were used as donor fluorophores, and mouse monoclonal anti-CDC42 antibody detected with secondary antibody labeled with Alexa 555 as acceptor fluorophore. The acceptor dye was photobleached using the 555 laser line (100% power, 70 iterations of 130 ms) at the membrane region. The energy transfer was detected as an increase in donor fluorescence (dequenching) after photobleaching the acceptor fluorophore. FRET efficiency was calculated as: (IDa-IDb)/IDa, IDa and IDb being the fluorescence intensity of the donor channel at the quenched area after and before the photobleaching, respectively. As a negative control, we used cells expressing GFP protein alone, stained for anti-CDC42 and secondary antibody labeled with Alexa 555. Additionally, FRET efficiency was calculated in areas of the same fields that were not subjected to photobleaching.

2.10. Statistical analysis

Data are expressed as the mean ± s.e.m. and are representative of at least three experiments. Paired Student's t-test was used for comparisons between experiments or for comparisons within each experiment when mixed populations of cells were used. Otherwise, non-parametric Mann–Whitney test was used for comparisons within each experiment. $p < 0.05$ was considered statistically significant.

2.11. Key resources table

Resource	Source	Identifier
Antibodies		
anti-pan-cytokeratin	Santa Cruz Biotechnology	#8018, C-11
mouse anti-CDC42	Santa Cruz Biotechnology	#8401, B-8
mouse anti-CIP4	BD Bioscience	#612556
mouse anti-GFP	Abcam	#ab290
mouse anti-g-tubulin	Sigma Aldrich	#T6557
mouse monoclonal anti-AKAP350	James Goldenring Lab	14G2
mouse monoclonal anti-E-cadherin	BD Bioscience	#610182
rabbit anti-cortactin-antibody	GeneTex	GTX100253
rabbit anti-Phospho-(-Ser/Thr) PKA substrate	Cell Signaling	#9621
CellLine		
HepG2/C3a	ATCC	HB-8065
MDA-MB-231	ATCC	HTB-26™
MDCK cells	Keith Mostov Lab	Madin–Darby Canine Kidney
Chemical		
pEGFP-N1	Clontech	6085–1
phalloidin-Alexa555	Thermo Fisher	A34055
pLPC	Giannino Del Sal lab	
ProteinPeptide		
CIP4	organism = "Homo sapiens"/db_xref = "taxon:9606"/ chromosome = "19"/ map = "19p13.3″	cdc42-interacting protein 4 isoform 2

3. Results

3.1. AKAP350 regulates CIP4 phosphorylation by PKA

To evaluate AKAP350 participation in CIP4 phosphorylation by PKA, we generated AKAP350 knocked down (AKAP350KD) cells by using a lentiviral system to express two different AKAP350 specific short hairpin RNAs (shRNA1 and shRNA4) (Supplementary Fig. 1A). The analysis of AKAP350 protein levels showed that, whereas the expression of both shRNAs efficiently decreased AKAP350 levels, shRNA1 was more effective than shRNA4 (shRNA1:-75%; shRNA4:-55%). Control and AKAP350KD cells were incubated in conditions of PKA activation, and the phosphorylation on CIP4 RXXS/T PKA consensus motifs was analyzed in CIP4 cell lysate immunoprecipitates by Western blot. Our results showed that CIP4 phosphorylation by PKA was severely impaired both in shRNA1 and shRNA4 AKAP350KD cells (Supplementary Fig. 1B). The analysis of three independent experiments performed with shRNA1 AKAP350 KD cells indicated a mean 70% decrease in PKA phosphorylated-CIP4 levels (Fig. 1). These results indicated that AKAP350 facilitates CIP4 phosphorylation by PKA.

3.2. CIP4 is phosphorylated by PKA on CIP4 T225

CIP4 interacts with the plasma membrane by means of its amino-terminal F-BAR domain, whereas its interaction with cdc42 and WASP is mediated by its HR1 and SH3 domains, respectively (Fig. 2A). To identify the specific site in the CIP4 sequence that is phosphorylated by PKA, we initially performed an *in silico* analysis using three different phosphorylation site prediction servers (see Materials and methods). The analysis revealed the presence of four putative PKA phosphorylation sites in the CIP4 sequence: T225, S296, S421 and S426. To determine which of these sites was actually phosphorylated, we generated expression plasmids for four CIP4 mutant versions where each amino acid was replaced by alanine, and performed *in vitro* phosphorylation assays using the recombinant proteins. Our results showed that, when

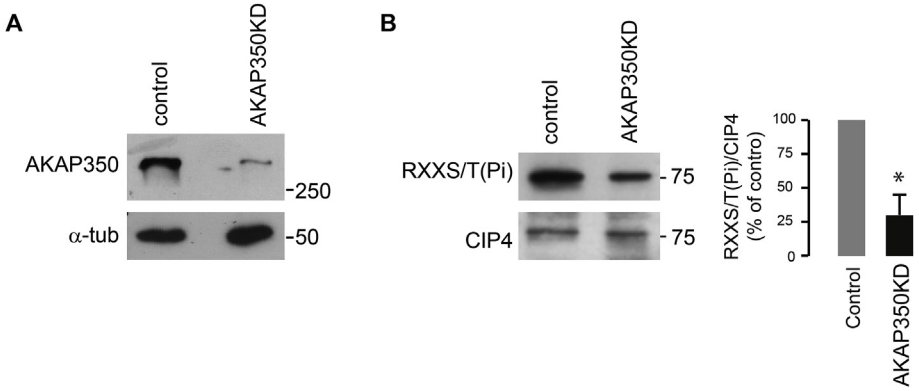

Fig. 1. Western blot analysis of CIP4 phosphorylation in control and AKAP350KD cells. (A) Cell lysates from MDCK cells transduced with shRNA1 (AKAP350KD) or scrambled shRNA1 (control) expressing lentiviral particles were resolved on 6% SDS-polyacrylamide gel electrophoresis, transferred to nitrocellulose membranes and analyzed by Western blot using mouse monoclonal anti-AKAP350 (14G2, 1:500) and anti-α-tubulin (Sigma-T9026, 1:3000) antibodies. (B) Control and AKAP350KD MDCK cells were incubated in the presence of 10 μm forskolin (Sigma) for 10 min, and lysed in the presence of phosphatase inhibitors. CIP4 immunoprecipitates were obtained from control and AKAP350KD cells using a mouse anti-CIP4 antibody and phosphorylation by PKA in the immunoprecipitates was analyzed by Western blot using an antibody that recognizes the RXXS/T(Pi) consensus motif (Supplementary methods). Bars indicate mean levels of RXXS/T(Pi) positive CIP4 levels, related to total CIP4 levels, expressed as percentage of controls of three independent experiments.

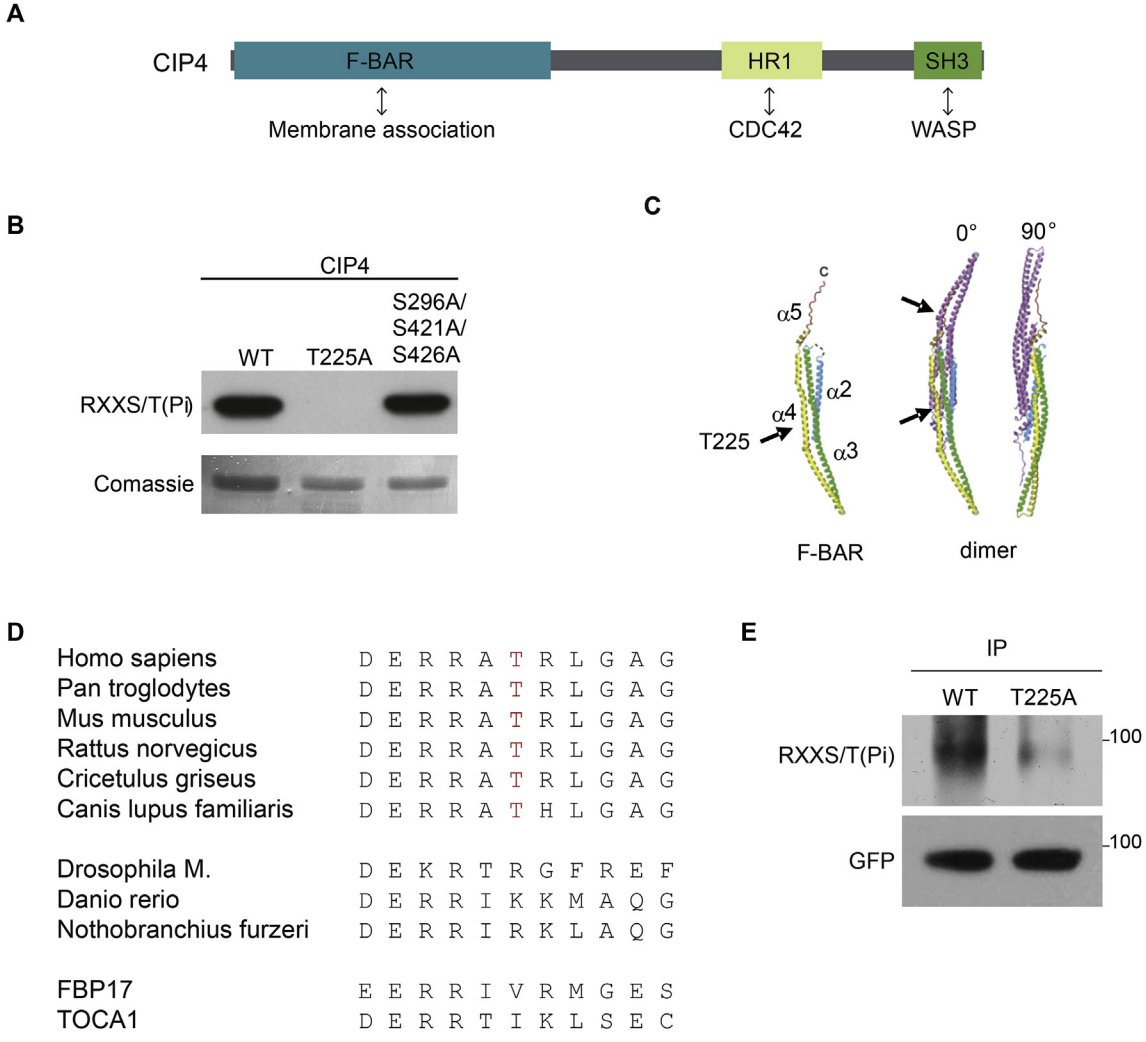

Fig. 2. PKA phosphorylates the CIP4 T225 residue, located in the CIP4 F-BAR domain. (A) Cartoon delineating CIP4 domains: F-BAR domain (CIP4 5-257), responsible for CIP4 dimerization and interaction with membrane phospholipids; cdc42 interacting domain (HR1, CIP4 395-475) and SH3 domain (CIP4 544-598). (B) *In vitro* phosphorylation. (His)6-tagged CIP4, CIP4(T225A) and CIP4(S296A/S421A/S426A) attached to Ni beads were incubated with the catalytic subunit of PKA as described [16]. The reactions were terminated by heating the samples in sample buffer at 65 °C for 20 min and analyzed by Western blot using a rabbit anti-RXXS/T(Pi) antibody as in Fig. 1 (C) 3-dimensional structure of the F-BAR domain crystal resolved by x-ray diffraction (https://www.ncbi.nlm.nih.gov/Structure/pdb/2EFK). The T225 residue localizes at the fourth α-helix in the convex side of the dimer. (D) Comparison of the CIP4 T225 sequence region in different species and in Homo sapiens CIP4-like proteins. (E) MDA-MB31 cells expressing CIP4WT-GFP and CIP4T225A-GFP proteins were exposed to 10 μM forskolin and lysed in the presence of protein phosphatase inhibitors. Fusion protein immunoprecipitates were obtained by using a mouse anti-GFP antibody and phosphorylation by PKA in the immunoprecipitates was analyzed by Western blot as in Fig. 2A.

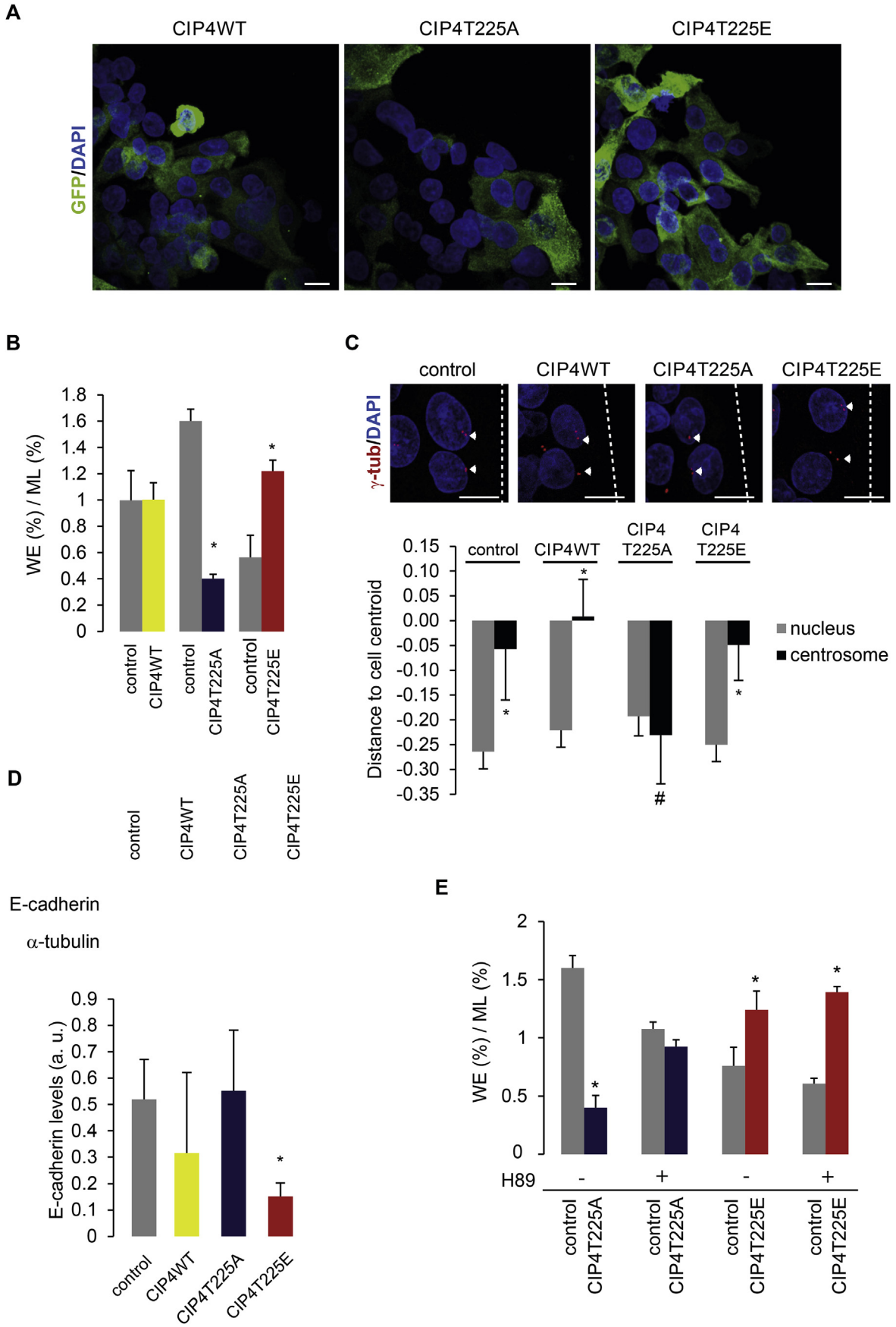

(caption on next page)

Fig. 3. Expression of CIP4(T225E) increases, whereas CIP4(T225A) inhibits, HepG2 migratory properties. (A) Equal amounts of control cells (not expressing GFP) and CIP4 WT, CIP4(T225A) or CIP4(T225E) cells were mixed and seeded to confluence to perform wound healing assays. Cells were fixed at 24 h and stained with DAPI for confocal microscopy. The amount of cells not expressing GFP (control) and cells expressing CIP4 fusion proteins at the wound edge (WE) and in the unperturbed confluent monolayer (ML) were determined. The images show cell distribution at the wound edge for each group. (B) Bars represent the average ratio between the percentages of cells in both locations for each group of cells. Data are expressed as means ± s.e.m. for at least 150 cells distributed in six separate fields for each location, representative of four independent experiments. *$p < 0.05$ compared to its control. (C) Cells were fixed 6 h after scratch wounding and stained using an anti-γ-tubulin antibody and DAPI for centrosome and nucleus visualization, respectively. Images were obtained by confocal microscopy and analyzed using ImageJ software. The difference between the distance from the centroid of the centrosome or the nucleus and the distance from the cell centroid to the line tangent to the leading edge was calculated and divided by the distance from the cell centroid to the leading edge. Negative values refer to organelle localization behind the cell centroid, whereas positive values indicate organelle localization in front of the cell centroid. Bar graph illustrates the position of the nucleus (gray) or the centrosome (black) in cells at the wound edge. Data are expressed as mean ± s.e.m. of at least 40 cells, representative of three independent experiments.*$p < 0.05$ compared to nucleus, $^{\#}p < 0.05$ compared to control. (D) Western blot analysis of E-cadherin expression in control, CIP4 WT, CIP4(T225A) and CIP4(T225E) cells. Cell lysates were prepared and analyzed by Western blot using mouse monoclonal anti-E-cadherin (BD Bioscience-610182, 1:1000) and monoclonal anti-alpha tubulin (Sigma-T9026, 1:3000) as loading control, as described.[13] Bars represent the mean E-cadherin expression relative to the loading control of three independent experiments. (E) Wound healing assays were performed as in A, in the absence or presence of the PKA inhibitor, H89 (1 μM), and quantified as in B. Data are expressed as mean ± s.e.m. of at least 150 cells distributed in six separate fields corresponding to each location, representative of three independent experiments. *$p < 0.05$ compared to control. Scale bars: 10 μm.

exposed to the PKA catalytic subunit, phosphorylation levels of CIP4(S296A), CIP4(S421A) and CIP4(S426A) mutants were similar to those of the wild-type protein (data not shown). Moreover, the triple mutant (S296, S421A, S426A) exhibited normal phosphorylation levels (Fig. 2B). In contrast, phosphorylation by PKA was completely absent in the CIP4(T225A) mutant (Fig. 2B), thus revealing this exclusive PKA phosphorylation site located within the CIP4 F-BAR domain. The *in silico* analysis of CIP4 quaternary structure, based on the resolution of the F-BAR domain crystal structure (https://www.ncbi.nlm.nih.gov/Structure/pdb/2EFK), revealed that T225 is positioned at the convex side of the F-BAR domain (Fig. 2C). Remarkably, we found that the T225 residue is highly conserved in mammals, although it is absent in zebrafish and other non-placental chordates and it is missing in the other CIP4-like proteins (formin-binding protein (FBP) 17 and transducer of CDC42-dependent actin assembly (TOCA) 1) (Fig. 2D). To evaluate if the CIP4 T225 residue is also a relevant PKA phosphorylation site at cellular level, we generated MDA-MB-231 cells with stable overexpression of CIP4 (CIP4WT) or CIP4(T225A) non-phosphorylatable mutant by transducing cells with pseudo-retroviral particles containing the constructs that code for their respective GFP fusion proteins. The expression of CIP4 chimeric proteins and the maintenance of endogenous CIP4 levels in the different cells were verified by Western blot (Supplementary Fig. 2). The phosphorylation of CIP4WT and CIP4T225A-GFP fusion proteins on RXXS/T sites was analyzed in conditions of PKA stimulation (Fig. 2E). Immunoprecipitates were prepared using an anti-GFP primary antibody, and RXXS/T phosphorylation was analyzed using anti-RXXS/T-Pi specific antibody, as described in Fig. 1. Our results showed that CIP4 WT was significantly immunoreactive, whereas the CIP4T225A mutant showed negligible immunoreactivity with the RXXS/T-Pi specific antibody. Considering our *in vitro* results, this low immunoreactive signal could be either a non-specific signal, or a different RXXS/T phosphorylation site that was phosphorylated less efficiently. These studies give strong support to the idea that CIP4 T225 is, at least, the prevalent CIP4 PKA phosphorylation site *in situ*.

3.3. Expression of a CIP4(T225E) phosphomimetic mutant increases the migratory efficiency in HepG2 cells

HepG2 are HCC-derived cells, which retain many of the epithelial characteristics of hepatocytes. Concomitantly, HepG2 cells are poorly invasive. Our previous studies showed that, when subjected to wound healing assays, the acquisition of a migratory phenotype in HepG2 cells depends on both CIP4 and AKAP350 expression [13]. Therefore, we evaluated the relevance of CIP4 phosphorylation by PKA to the acquisition of migratory and invasive properties in HepG2 cells. We prepared HepG2 cells with stable expression of CIP4 (CIP4WT), the CIP4(T225E) phosphomimetic or the CIP4(T225A) non-phosphorylatable mutants as GFP fusion proteins. The analysis of CIP4 fusion proteins expression by Western blot showed that protein levels did not differ significantly among mutants (Supplementary Fig. 3). Considering the low migratory efficiency of HepG2 cells, we performed experimental wound healing assays using a mixed population of cells that contained equal numbers of CIP4(T225E) or CIP4(T225A) and control cells. After 24 h, we calculated the ratio for each group of cells at the wound edge (Fig. 3A) and compared it to the ratio of cells that were located in the monolayer, far from the wound edge. As compared to traditional wound healing assays, this method allows higher sensitivity for determining changes in directional cell migration efficiency and avoids artifacts originating in differences in cell proliferation rates [13]. Our results showed that, compared to control cells, the migratory efficiency was doubled in CIP4(T225E), and reduced to 25% in CIP4(T225A) cells (Fig. 3 B), demonstrating an eight-fold increase in the migratory efficiency for cells expressing the phosphomimetic mutant with respect to the cells expressing the non-phosphorylatable mutant. On the other hand, we did not observe any difference in directional cell migration efficiency between control and CIP4WT cells. Directional cell migration requires the asymmetric reorganization of the cell components in order to acquire a front–rear polarity, which ensures the directional trafficking of membranes and regulatory proteins towards the leading edge. The acquisition of this migratory polarity involves nucleus movement to the back and centrosomal relocation to the front of the nucleus [26]. Concurrently, the analysis of centrosome position relative to the nucleus in HepG2 cells showed that the acquisition of a migratory phenotype was impaired by the expression of CIP4(T225A) (Fig. 3C). An initial event in the acquisition of the migratory phenotype in epithelial cells is the disruption of adherens junctions by E-cadherin endocytosis and degradation. Considering that E-cadherin endocytosis can be regulated by CIP4, E-cadherin protein levels in the different cell populations were analyzed by Western blot. In accordance with the wound healing results, E-cadherin levels were significantly decreased in CIP4(T225E) cells, but were unaffected in CIP4(T225A) cells (Fig. 3D). In CIP4WT-expressing cells, there was a subtle decrease in E-cadherin levels that was not statistically significant. This is consistent with previous studies from other authors, who showed that, whereas CIP4 overexpression is associated with E-cadherin endocytosis, total levels of E-cadherin were not affected by changes in CIP4 expression [8]. Taking everything into account, these results indicate that CIP4 T225 phosphorylation is a regulatory event relevant to the acquisition of the mesenchymal, migratory phenotype in HepG2 cells.

Our recent studies have demonstrated that PKA inhibition decreased HepG2 migratory efficiency in wound healing assays [27]. We performed wound healing assays in mixed populations of control and CIP4 T225 mutant cells in basal conditions and in the presence of the PKA inhibitor, H89 (Fig. 3E). PKA inhibition eliminated the differences in migratory efficiency between control and CIP4(T225A) cells and, conversely, potentiated the migratory advantage conferred by the

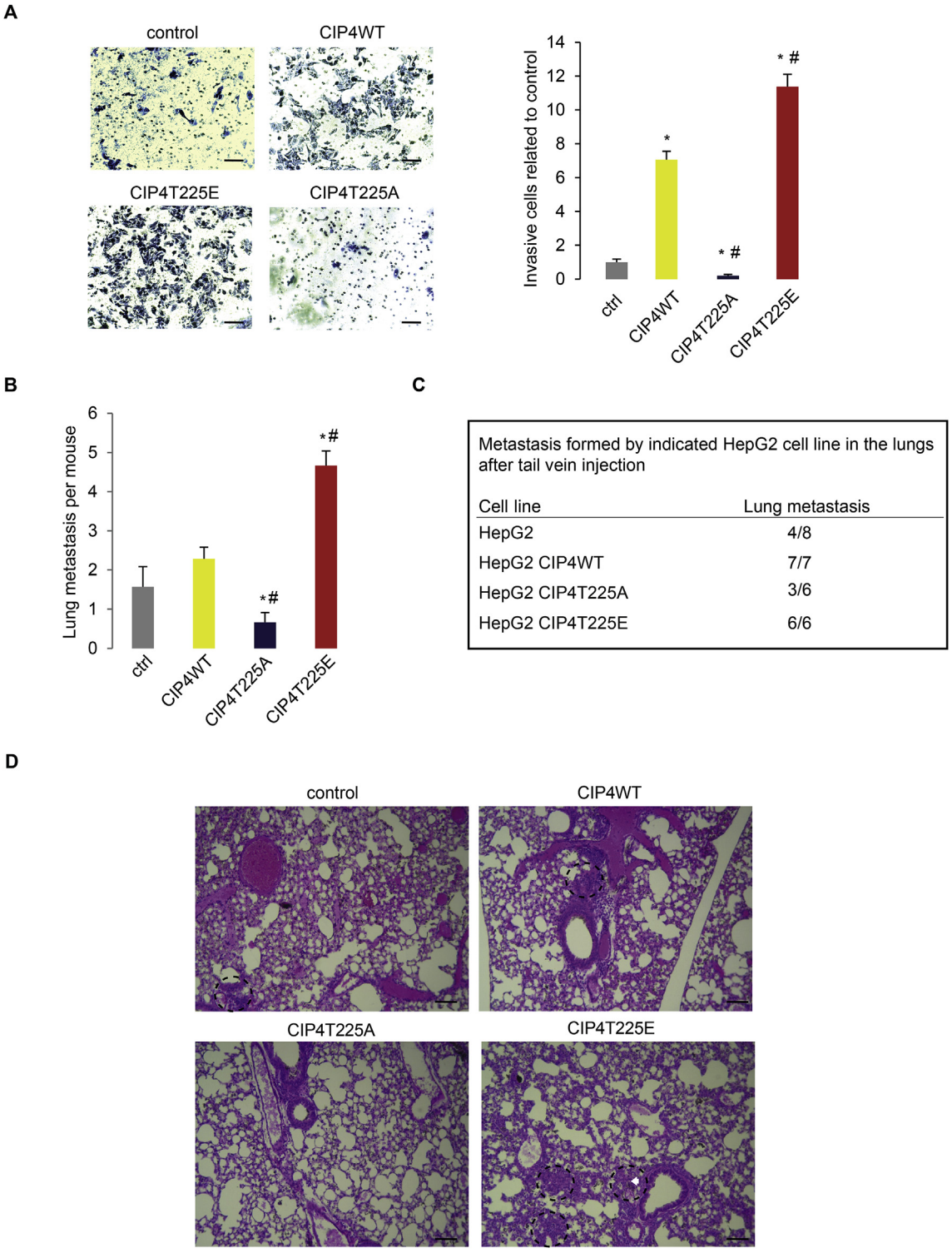

Fig. 4. Phosphorylation at CIP4 T225 modulates HepG2 invasive capacity *in vitro* and metastasis *in* vivo. (A) Invasion assays in Boyden chambers. Invasion capacity was assessed for the different cell lines using Matrigel-coated transwells. Cells were seeded into the upper chamber and incubated for 48 h. Cells in the upper chamber were removed and the remaining cells were fixed and stained for optical microscopy. Bars represent the ratio of cells that invaded into the lower chamber for each cell line related to control cells, quantified in ten different fields for three independent experiments. *p < 0.05 compared to control. #p < 0.05 compared to CIP4 WT. (B-D) Experimental metastasis assay. Control HepG2, CIP4 WT, CIP4(T225A) or CIP4(T225E) cell lines were injected via the tail vein into athymic nude mice. After 8 weeks, animals were sacrificed and the lungs were fixed and stained with ink to visualize metastatic nodules by counterstaining and direct fluorescence. (B) Bars represent the number of metastases observed per lung for each group. *p < 0.05 compared to control. #p < 0.05 compared to CIP4 WT. (C) The table shows the number of mice that developed lung metastases after tail vein injection of the indicated HepG2 cells. The x/y ratio indicates the number of animals that scored positive metastases in lung (x) versus the total number of mice analyzed in the experiments (y). (D) Representative images of hematoxylin and eosin staining of lung tissue from athymic nude mice injected with the different cell lines showing metastatic foci of cancer cells (black circles). Scale bars: 50 μm (A), 100 μm (D).

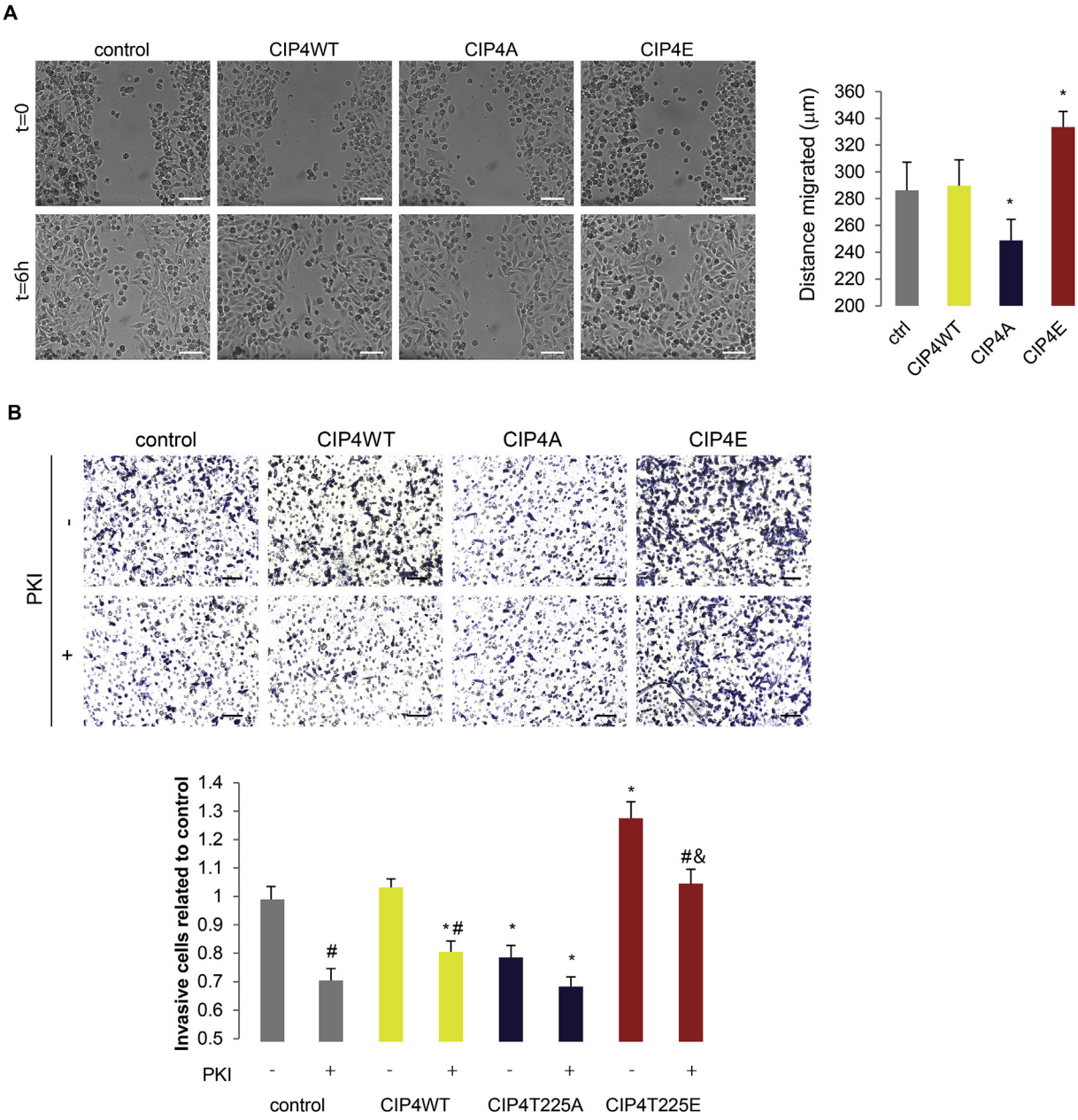

Fig. 5. Expression of CIP4(T225E) increases, whereas CIP4(T225A) represses, MDA-MB-231 migratory and invasive properties. (A) Wound healing assays performed in MDA-MB231 cells expressing CIP4 WT, CIP4(T225A) or CIP4(T225E). Cells were seeded 24 h before the experiment, the intact monolayer was scratched, and cells were allowed to migrate for 6 h. Images of the same field acquired at 0 and 6 h were analyzed using the ImageJ software. Bars represent the average distance migrated in µm by each cell line. *p < 0.01 compared to control. (B) Representative images of invasion assays in Boyden chambers. Cell invasiveness was studied using Matrigel coated transwells. Cells were seeded into the upper chamber and incubated with or without PKI. After 24 h, cells in the upper chamber were removed and the remaining cells were fixed and stained with toluidine blue for optical microscopy. Bars represent the ratio of cells that invaded the lower chamber related to control cells. *p < 0.01 compared to control PKI (−). $^{\&}$p < 0.01 compared to control PKI (+). $^{\#}$p < 0.01 PKI (−) compared to PKI (+) within the same group. Data are expressed as mean ± s.e.m. of at least eight (A) or ten (B) fields, representative of three independent experiments. Scale bars: 50 µm (A,B). (For interpretation of the references to color in this figure legend, the reader is referred to the Web version of this article.)

expression of the CIP4(T225E) mutant. These results highlight the significance of CIP4 T225 phosphorylation for PKA regulatory effect on HepG2 cell migration.

3.4. Expression of the CIP4(T225E) phosphomimetic mutant enhances HepG2 cell invasiveness

We further analyzed the relevance of CIP4 T225 phosphorylation to HepG2 cell invasiveness using *in vitro* and *in vivo* assays. Our *in vitro* experiments performed in Matrigel-coated permeable transwells showed that expression of the CIP4(T225E) mutant markedly increased the number of cells invading the lower chamber (+1100%), as opposed to the expression of the CIP4(T225A) mutant, which severely impaired cell invasiveness (−90%) (Fig. 4A). Likewise, experimental metastasis experiments performed by injecting control, CIP4 WT, CIP4(T225E) or CIP4(T225A) HepG2 cells into the tail vein of athymic nude mice, showed that, compared to CIP4 WT cells, CIP4(T225E) cells were much more efficient, whereas CIP4(T225A) cells were significantly less efficient in generating metastatic nodules (Fig. 4B and C). The analysis of the hematoxylin and eosin staining of the lungs (Fig. 4D) and the

A

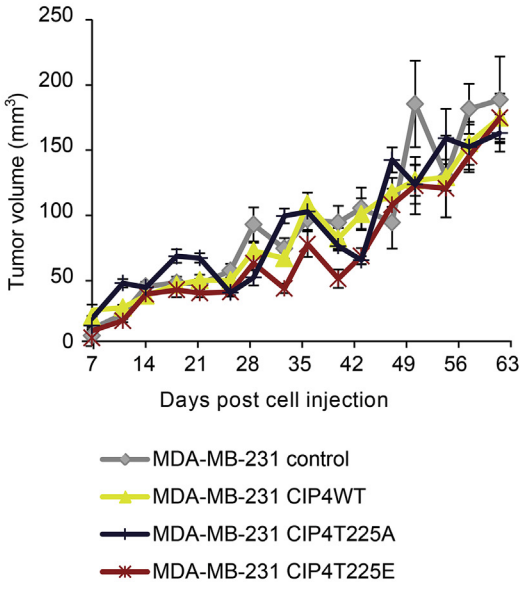

B

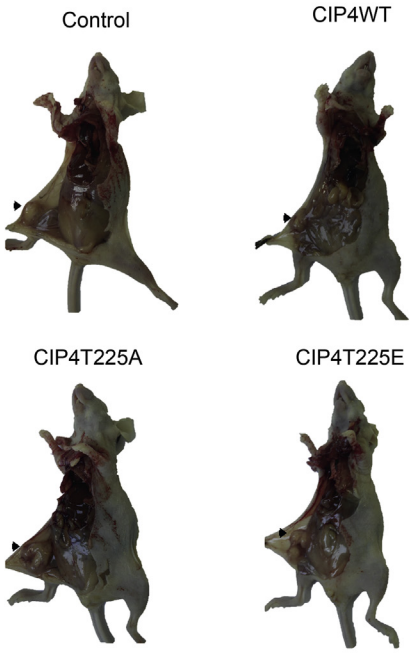

C

Metastasis formed by indicated MDA-MB-231 cell line in the lungs on orthotopic transplantation in mammary pads.

Cell line	Lung metastasis
MDA-MB-231	2/4
MDA-MB-231 CIP4WT	5/7
MDA-MB-231 CIP4T225A	2/8
MDA-MB-231 CIP4T225E	7/7

D

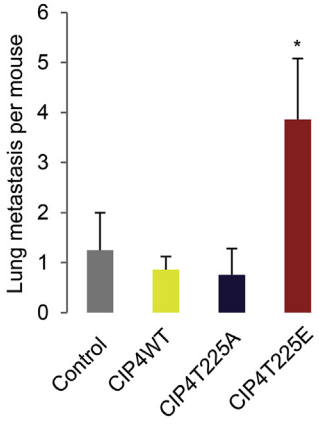

E

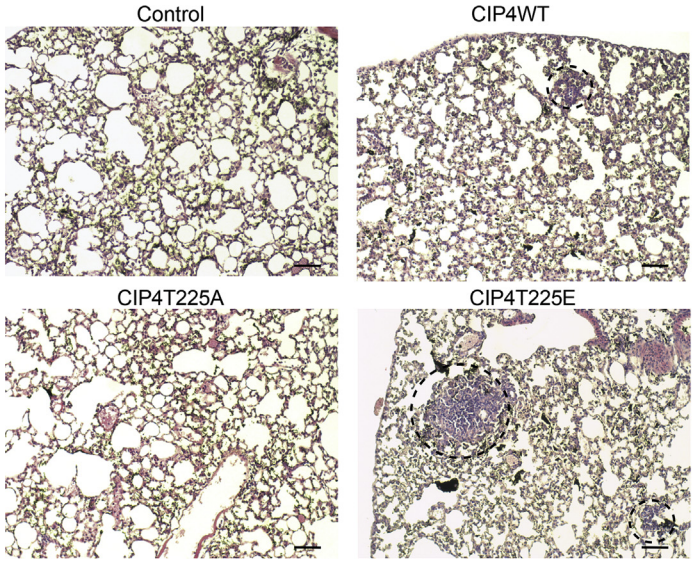

(caption on next page)

Fig. 6. Expression of the CIP4(T225E) phosphomimetic mutant promotes spontaneous metastasis in MDA-MB-231 orthotopic xenografts. Fifty µl of a suspension containing 1 x 10^6 MDA-MB-231 cells in a 50:50 solution of Matrigel/PBS was introduced into the right inguinal mammary gland of anaesthetized, 6-week-old female athymic nude mice. (A) Primary tumor growth was estimated by measuring tumor length (a) and width (b) every 3-4 days, and tumor volume (V) was calculated using the formula $V = 0.4\,ab^2$. (B) After 12 weeks, mice were euthanized, the chest cavity was exposed through a midline chest incision and the presence of the primary tumors was corroborated by direct visualization. (C) The trachea was cannulated, and lungs inflated using 1 ml of Indian ink. Lungs were then extracted and destained, and metastatic nodules counted *de visu*. The x/y ratio indicates the number of mice that scored positive for metastasis (x) versus the total number analyzed in the experiments (y) for the different groups of mice. (D) Bars represent the number of metastases formed in the lungs per mouse by each indicated MDA-MB-231 cell line. (E) Representative images of hematoxylin and eosin staining of lung tissue from athymic nude mice injected with the indicated cells showing metastatic foci of cancer cells (black circles). Scale bars: 100 µm.

immunohistochemical staining for cytokeratins in lung proximal lymphatic nodes (Supplementary Fig. 4) were consistent with these observations. Overall, these results indicate that CIP4 T225 phosphorylation is a central event in the regulation of HCC cell metastatic properties.

3.5. CIP4 T225 phosphorylation participates in the acquisition of MDA-MB-231 cell migratory and invasive properties

MDA-MB-231 cells are triple negative breast cancer cells, whose highly metastatic properties rely, at least partially, on their elevated CIP4 levels [7]. Hence, we analyzed the relevance of CIP4 T225 phosphorylation to MDA-MB-231 cell acquisition of migratory and invasive properties. MDA-MB-231 cells with stable expression of CIP4WT, CIP4(T225A) and CIP4(T225E) mutants were generated as explained above. Wound-healing assays performed on these cell lines showed that CIP4(T225A) expression significantly inhibited, whereas CIP4(T225E) expression significantly increased, the efficiency of directional cell migration in MDA-MB-231 cells (Fig. 5A), indicating that the presence of the phosphomimetic residue in this position gave a migratory advantage to these cells.

Previous studies demonstrated that the activation of PKA increases MDA-MB-231 cell invasiveness [28]. We analyzed the effect of the expression of CIP4 T225 mutants on cell invasiveness in basal conditions and in the presence of the PKA inhibitory peptide, PKI. *In vitro* invasion assays showed that CIP4(T225A) cells were less invasive whereas CIP4(T225E) cells were significantly more invasive than control or CIP4 WT-expressing cells (Fig. 5B). The presence of the PKA inhibitor (PKI) decreased control and CIP4 WT cell invasiveness to CIP4(T225A) levels, without modifying CIP4(T225A) cell invasiveness. On the other hand, although CIP4(T225E) cell invasiveness was inhibited in the presence of PKI, it still remained significantly higher than control or CIP4 WT cells in the same conditions. These results reveal that CIP4 T225 is a significant PKA substrate in the pathway regulating cell invasiveness in triple negative breast cancer cells.

3.6. Expression of the CIP4(T225E) phosphomimetic mutant promotes spontaneous metastasis in MDA-MB-231 orthotopic xenografts in athymic nude mice

To test whether CIP4 T225 phosphorylation regulates tumor progression and metastasis, MDA-MB-231 cells were orthotopically injected into the mammary fat pad of athymic nude mice. Overexpression of CIP4 WT or expression of CIP4(T225A) or CIP4(T225E) mutants did not affect tumor growth (Fig. 6A and B). On the other hand, CIP4 overexpression enhanced spontaneous metastasis (Fig. 6C). Furthermore, we observed that mice injected with cells expressing the CIP4(T225E) phosphomimetic mutant developed lung nodules at an even higher frequency, considering both the number of mice that developed metastasis (Fig. 6C) and the number of metastatic nodules in each individual mice (Fig. 6D). In contrast, mice inoculated with CIP4(T225A) cells rarely developed lung metastasis (Fig. 6C and D). The analysis of the hematoxylin and eosin staining of the lungs supported these observations (Fig. 6E). Similarly, the analysis of the immunohistochemical staining for cytokeratins in lung proximal lymphatic nodules revealed the presence of an increased number of cytokeratin positive cells in mice injected with CIP4(T225E) cells when compared to mice injected with CIP4 WT or CIP4(T225A) cells (Supplementary Fig. 5).

3.7. Expression of the CIP4 T225 non-phosphorylatable mutant decreases CIP4 interaction with CDC42 at the cell edge and inhibits invadopodia formation

CIP4 enhancement of triple negative breast cancer cell invasiveness is, at least in part, due to its role in invadopodia formation. We analyzed the formation of functional invadopodia in MDA-MB-231 CIP4 WT, CIP4(T225A) and CIP4(T225E) cells grown on coverslips coated with FITC-conjugated gelatin. Functional invadopodia were identified as actin/cortatctin positive structures in contact with the ECM that were able to degrade gelatin. Our results showed that expression of CIP4(T225A) inhibited, whereas expression of CIP4(T225E) slightly increased the generation of functional invadopodia (Fig. 7A–C).We further analyzed the subcellular localization of the CIP4 T225 mutants. Invadopodia visualization in the orthogonal views of the image stacks showed that, as previously described, CIP4 was enriched at such structures [7]. Compared to CIP4 WT, CIP4(T225E) levels at invadopodia were significantly higher, whereas CIP4(T225A) localization at these structures was not so prominent (Fig. 7D).

Considering that the role of CIP4 in invadopodia formation is dependent on its interaction with CDC42, we analyzed if CIP4 T225 phosphorylation was relevant for this interaction. We analyzed the *in situ* CIP4/CDC42 interaction at the cell edge in MDA-MB-231 CIP4 WT and CIP4(T225A) cells using immuno FRET by acceptor photobleaching. Cells that expressed GFP alone were used as negative controls. Our results showed that, even when both CIP4 WT and CIP4(T225A) interacted with CDC42, the T225A mutation significantly decreased FRET efficiency (-43%, $p < 0.05$), indicating that CIP4/CDC42 interaction was inhibited by the presence of a non-phosphorylatable amino acid in the T225 position (Fig. 7E). We did not observe any significant difference in FRET efficiency between CIP4(T225E)/CDC42 and CIP4(T225WT)/CDC42 donor/acceptor pairs (data not shown).

4. Discussion

During disease progression, cancer cells are exposed to conditions that impose severe limitations on proliferation and survival. Therefore, the capacity to dynamically regulate cell behavior gives cells an important advantage, particularly during metastatic spread. Phosphorylation is a common reversible mechanism for triggering or inhibiting the activity of specific proteins in a signaling pathway. Hence, it is not surprising that altered phosphorylation of key proteins participates in oncogenic mechanisms. Specifically, PKA plays a regulatory role in cancer initiation and progression by either enhancing or inhibiting proliferation and dissemination of malignant cells in a cancer-dependent manner [20,29]. PKA is a serine/threonine kinase whose interaction with its scaffolding proteins by means of its regulatory domain determines its accessibility to specific substrates [30]. In this regard, the traditional model proposes that, upon cAMP interaction with the regulatory subunit, PKA catalytic subunits are activated and released from the complex. Nevertheless, recent studies have

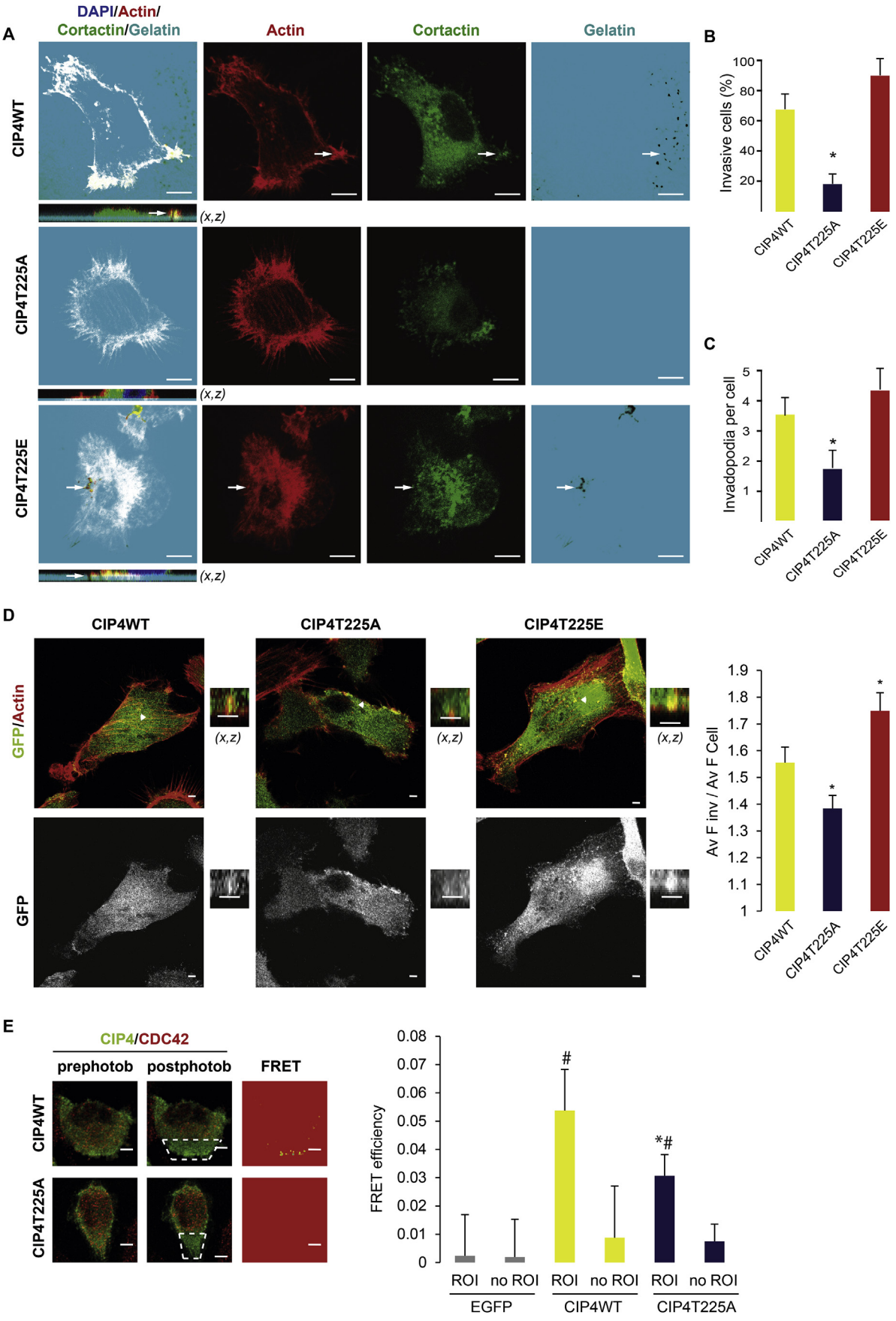

(caption on next page)

Fig. 7. CIP4 T225 phosphorylation affects the formation of functional invadopodia and CIP4 interaction with CDC42. (A) Cells were incubated on coverslips coated with gelatin conjugated to FITC for 16 h at 37 °C and then fixed and stained with phalloidin-Alexa 555 and anti-cortactin-antibody. Foci of degraded matrix were visible as dark areas of 0.2–1.2 μm in diameter in the bright fluorescent gelatin matrix (arrows). Images show DAPI (blue), actin (red) and cortactin (green) staining and FITC-gelatin (cyan). *x,z* Orthogonal views are shown below each *x,y* merged image. (B) A cell generating at least one "hole" under the cell or near the cell edge was counted as a cell able to degrade matrix (invasive cell). Bars represent the number of invasive cells, expressed as percentage of total cells for each cell line. *p < 0.05 compared to CIP4 WT and CIP4(T225E). (C) Functional invadopodia were identified as actin- and cortactin-rich structures localized close to foci of degraded matrix. Bars represent the total number of invadopodia per invasive cell for each cell line. *p < 0.05 compared to CIP4 WT and CIP4(T225E). (D) Cells were seeded on matrigel coated coverslips, incubated for 16 h and then fixed and stained with phalloidin for confocal microscopy. Invadopodia were identified as actin dots, positive for CIP4-GFP fluorescence, in contact with the ECM. Merged images show the visualization of CIP4 (green) and actin (red) staining in MDA-MB 231 cells expressing CIP4 WT, CIP4(T225A) or CIP4(T225E). White arrowheads indicate representative invadopodia. The panels below each *x,y* image show the *x,z* magnified views of a representative invadopodia. Bars represent average GFP intensities measured at invadopodia (Av F_{inv}) related to the average GFP intensity in the cell (Av F_{cell}) for each construct. Data are expressed as mean ± s.e.m. of at least thirty cells, representative of three independent experiments. *p < 0.05 compared to CIP4 WT. (E) Confocal images of MDA-MB 231 cells expressing CIP4-GFP fusion constructs and stained for CDC42 using a secondary antibody bound to Alexa 555. Delimited areas represent the photobleached regions. Briefly, a region of interest (ROI) which included the cell edge was photobleached at 555 nm wavelength and images were taken before and after photobleaching. Total GFP fluorescence in that ROI was measure before and after acceptor photobleaching to assess FRET efficiency as described in the materials and methods. FRET efficiency was also calculated for MDA-MB 231 cells expressing GFP and stained for CDC42, and for each image outside the photobleached ROI (no ROI) (negative controls). FRET images show the difference in GFP fluorescence after and before acceptor photobleaching, represented in pseudocolor. Bars represent the FRET efficiency calculated for each cell line. Data are expressed as mean ± s.e.m. of ten photobleached areas, representative of three independent experiments.*p < 0.05 compared to CIP4WT (ROI). #p < 0.01 compared ROI vs. no ROI in the same group. Scale bars: 5 μm (A, E) or 2,5 μm (D). (For interpretation of the references to color in this figure legend, the reader is referred to the Web version of this article.)

proposed that increases in cAMP within physiological levels activate PKA without inducing the separation of the catalytic subunit [31]. Therefore, protein phosphorylation is much more regionally confined than previously appreciated and it is restricted to substrates within the immediate vicinity of PKA scaffolded by particular AKAPs. Accordingly, recent studies have demonstrated that interference with the interaction between PKA and its anchoring proteins impairs PKA-mediated tumorigenesis in mammary epithelial cells [32,33]. CIP4 is a PKA substrate which interacts with the PKA anchoring protein AKAP350 [16]. In the present study, we found that CIP4 phosphorylation by PKA is dependent on AKAP350 expression and we identified CIP4 T225 as the exclusive CIP4 PKA phosphorylation site. Considering that different lines of evidence suggest a functional interaction between CIP4 and AKAP350 during the acquisition of invasive properties [13,19], we hypothesized that CIP4 T225 phosphorylation by PKA regulates CIP4 function during the development of invasive properties in cancer cells.

In spite of its pro-invasive effects in breast cancer, osteosarcoma, nasopharyngeal and small lung cancer cells, CIP4 overexpression leads to decreased cell migration and invasion in NIH 3T3 fibroblastic cells [15]. Moreover, *in vitro* experiments performed in MDA-MB-231 cells showed that CIP4 Y471 phosphorylation by Src could induce an anti-invasive effect of CIP4 [14]. In the present study, we provide evidence that CIP4 phosphorylation at CIP4 T225 by PKA enhances its pro-invasive activity both in HCC and in triple negative breast cancer cells: First, in HepG2 cells, expression of the CIP4(T225E) phosphomimetic mutant decreased E-cadherin protein levels, whereas expression of the CIP4(T225A) non-phosphorylatable mutant inhibited the acquisition of a migratory phenotype. Second, expression of CIP4(T225E) increased, whereas expression of CIP4(T225A) decreased the migratory efficiency and invasiveness in HepG2 and MDA-MB-231 cells. Concomitantly, CIP4(T225A) expression inhibited the capacity of MDA-MB-231 cells to develop functional invadopodia. Third, experiments in athymic mice showed that HepG2 and MDA-MB-231 cells expressing the phosphomimetic mutant were more prone to develop lung metastases. Fourth, the promigratory and proinvasive effects of PKA in HepG2 and MDA-MB-231 cells were prevented by the presence of the CIP4(T225A) non-phosphorylatable mutant, which indicates that CIP4 constitutes an important substrate in the signaling pathways involving PKA as a tumor-promoting kinase.

CIP4 participation in cell acquisition of migratory and invasive properties is linked to its role as a CDC42 effector in coordinating actin cytoskeleton remodeling and membrane deformation. Those processes are essential for E-cadherin endocytosis as well as for the formation of membrane cell protrusions during the initial phases of cell migration and invasion [4,34]. The role of CIP4 in membrane deformation is reliant on the direct interaction of its F-BAR domain with the membrane [2], whereas its participation in actin nucleation depends on its simultaneous interaction with active CDC42 and N-WASP [1,3,4]. N-WASP interaction with active CDC42 is essential for the generation of its "open" conformation, which promotes actin nucleation [35,36]. In this scenario, by directly interacting with N-WASP and active CDC42, CIP4 acts as a membrane bound scaffold that facilitates N-WASP activation [7]. CIP4 interacts with active CDC42 by means of its HR1 domain, located C-terminal to the F-BAR domain (Fig. 1A) [1]. FRET analysis of MB-231 CIP4 WT and CIP4(T225A) cells showed that mutation of CIP4 T225 to the non-phosphorylatable amino acid alanine inhibited CIP4 interaction with CDC42 at the cell edge. Thus, CIP4 interaction with CDC42 was dependent on CIP4 T225 phosphorylation. We have not been able to verify these *in situ* findings by biochemical assays, because we could not co-immunoprecipitate endogenous CDC42 with CIP4. This is most likely related to the fact that CIP4 HR1 domain (as well as FBP17 and TOCA-1 HR1 domains) has a remarkably low affinity for CDC42. *In vivo,* this makes their interaction dependent on the compartmentalization of both proteins at the membrane, which is lost under immunoprecipitation conditions [37]. Therefore, CIP4 phosphorylation could favor cell migration and invasion by increasing its interaction with active CDC42 at the membrane, hence regulating actin nucleation at membrane protrusions. In accordance with our hypothesis, we found that expression of the CIP4(T225A) mutant inhibited invadopodia formation. In addition, CIP4 localization at invadopodia was enhanced by the presence of the phosphomimetic mutation, but was decreased by the presence of the non-phosphorylatable mutant. At this point, a relevant question is: How does CIP4 T225 phosphorylation regulate the protein localization to invadopodia? CIP4 T225 is positioned at the convex side of F-BAR domain, whereas its concave surface is the one responsible for CIP4 interaction with the plasma membrane [38]. Therefore, it is not likely that T225 phosphorylation directly affects CIP4 interaction with plasma membrane phospholipids. Previous studies indicated that constitutively active CDC42 can modulate CIP4 localization at the cell edge [1]. We might speculate that decreased localization of CIP4 to invadopodia could be related to its decreased interaction with CDC42. Nevertheless, studies performed in cortical neurons showed that the CIP4 HR1 domain barely affected CIP4 localization to protruding membranes, indicating that direct interaction with CDC42 was dispensable for CIP4 localization at those structures [39]. Instead, the decrease in CIP4 interaction with CDC42 could be the consequence of its decreased ability to localize to invadopodia. The F-BAR domain is also responsible for CIP4 dimerization. Considering that CIP4 interaction with the plasma membrane is dependent on its dimerization, future studies will focus on elucidating if

CIP4 T225 phosphorylation has a direct impact on CIP4 dimerization and interaction with the plasma membrane and/or on its ability to directly interact with CDC42.

Conflicts of interest

The authors declare no conflict of interest.

CRediT authorship contribution statement

Facundo M. Tonucci: Methodology, Investigation, Data curation. **Evangelina Almada:** Methodology, Investigation. **Carla Borini-Etichetti:** Methodology, Investigation. **Alejandro Pariani:** Methodology, Investigation. **Florencia Hidalgo:** Methodology, Investigation. **M. Jose Rico:** Methodology, Investigation. **Javier Girardini:** Supervision, Writing - review & editing. **Cristián Favre:** Supervision, Writing - review & editing. **James R. Goldenring:** Resources, Conceptualization, Methodology, Supervision, Writing - review & editing. **Mauricio Menacho-Marquez:** Conceptualization, Methodology, Supervision, Writing - review & editing. **M. Cecilia Larocca:** Resources, Funding acquisition, Conceptualization, Methodology, Investigation, Supervision, Writing - original draft, Writing - review & editing.

Acknowledgements

This work was supported by Agencia Nacional de Promoción Científica y Tecnológica (PICT2015-2755 to M.C.L.) and CONICET (PUE2016 to IFISE). We would like to thank Prof. Liliana Rodriguez and the staff from the English Department of the Facultad de Ciencias Bioquímicas y Farmacéuticas (UNR) for the language correction of the manuscript, Alejandra Martinez (Fac. Cs. Bioq. Farm.-UNR) for her expert assistance in immunhistochemical analysis of mice lungs and Rodrigo Vena (Instituto de Biología Molecular y Celular de Rosario-CONICET) for his technical assistance in FRET experiments.

Appendix A. Supplementary data

Supplementary data to this article can be found online at https://doi.org/10.1016/j.canlet.2019.07.006.

References

[1] P.A. Aspenström, Cdc42 target protein with homology to the non-kinase domain of FER has a potential role in regulating the actin cytoskeleton, Curr. Biol. 7 (1997) 479–487.
[2] R.H. Roberts-Galbraith, K.L. Gould, Setting the F-BAR: functions and regulation of the F-BAR protein family, Cell Cycle 9 (2010) 4091–4097.
[3] L. Tian, D.L. Nelson, D.M. Stewart, Cdc42-interacting protein 4 mediates binding of the Wiskott-Aldrich syndrome protein to microtubules, J. Biol. Chem. 275 (2000) 7854–7861.
[4] R. Fricke, C. Gohl, E. Dharmalingam, A. Grevelhörster, B. Zahedi, N. Harden, et al., Drosophila Cip4/Toca-1 integrates membrane trafficking and actin dynamics through WASP and SCAR/WAVE, Curr. Biol. 19 (2009) 1429–1437.
[5] K. Tsujita, S. Suetsugu, N. Sasaki, M. Furutani, T. Oikawa, T. Takenawa, Coordination between the actin cytoskeleton and membrane deformation by a novel membrane tubulation domain of PCH proteins is involved in endocytosis, J. Cell Biol. 172 (2006) 269–279.
[6] P. Aspenström, N. Richnau, A.S. Johansson, The diaphanous-related formin DAAM1 collaborates with the Rho GTPases RhoA and Cdc42, CIP4 and Src in regulating cell morphogenesis and actin dynamics, Exp. Cell Res. 312 (2006) 2180–2194.
[7] C.S. Pichot, C. Arvanitis, S.M. Hartig, S.A. Jensen, J. Bechill, S. Marzouk, et al., Cdc42-interacting protein 4 promotes breast cancer cell invasion and formation of invadopodia through activation of N-WASp, Cancer Res. 70 (2010) 8347–8356.
[8] Y. Rolland, P. Marighetti, C. Malinverno, S. Confalonieri, C. Luise, N. Ducano, et al., The CDC42-interacting protein 4 controls epithelial cell cohesion and tumor dissemination, Dev. Cell 30 (2014) 553–568.
[9] P. Truesdell, J. Ahn, H. Chander, J. Meens, K. Watt, X. Yang, A.W. Craig, et al., CIP4 promotes lung adenocarcinoma metastasis and is associated with poor prognosis, Oncogene 34 (2015) 3527–3535.
[10] N.V. Koshkina, G. Yang, E.S. Kleinerman, Inhibition of Cdc42-interacting protein 4 (CIP4) impairs osteosarcoma tumor progression, Curr. Cancer Drug Targets 13 (2013) 48–56.
[11] O.L. Cerqueira, P. Truesdell, T. Baldassarre, S.A. Vilella-Arias, K. Watt, J. Meens, et al., CIP4 promotes metastasis in triple-negative breast cancer and is associated with poor patient prognosis, Oncotarget 6 (2015) 9397–9408.
[12] D.F. Meng, P. Xie, L.X. Peng, R. Sun, D.H. Luo, Q.Y. Chen, et al., CDC42-interacting protein 4 promotes metastasis of nasopharyngeal carcinoma by mediating invadopodia formation and activating EGFR signaling, J. Exp. Clin. Cancer Res. 36 (2017) 21.
[13] F.M. Tonucci, F. Hidalgo, A. Ferretti, E. Almada, C. Favre, J.R. Goldenring, et al., Centrosomal AKAP350 and CIP4 act in concert to define the polarized localization of the centrosome and Golgi in migratory cells, J. Cell Sci. 128 (2015) 3277–3289.
[14] J. Hu, A. Mukhopadhyay, P. Truesdell, H. Chander, U.K. Mukhopadhyay, A.S. Mak, et al., Cdc42-interacting protein 4 is a Src substrate that regulates invadopodia and invasiveness of breast tumors by promoting MT1-MMP endocytosis, J. Cell Sci. 124 (2011) 1739–1751.
[15] P. Dombrosky-Ferlan, A. Grishin, R.J. Botelho, M. Sampson, L. Wang, W.A. Rudert, et al., Felic (CIP4b), a novel binding partner with the Src kinase Lyn and Cdc42, localizes to the phagocytic cup, Blood 101 (2003) 2804–2809.
[16] M.C. Larocca, R.A. Shanks, L. Tian, D.L. Nelson, D.M. Stewart, J.R. Goldenring, AKAP350 interaction with cdc42 interacting protein 4 at the Golgi apparatus, Mol. Biol. Cell 15 (2004) 2771–2781.
[17] B. Frank, M. Wiestler, S. Kropp, K. Hemminki, A.B. Spurdle, C. Sutter, et al., Association of a common AKAP9 variant with breast cancer risk: a collaborative analysis, J. Natl. Cancer Inst. 100 (2008) 437–442.
[18] O. Kabbarah, C. Nogueira, B. Feng, R.M. Nazarian, M. Bosenberg, M. Wu, et al., Integrative genome comparison of primary and metastatic melanomas, PLoS One 5 (2010) e10770.
[19] Z.Y. Hu, Y.P. Liu, L.Y. Xie, X.Y. Wang, F. Yang, S.Y. Chen, et al., AKAP-9 promotes colorectal cancer development by regulating Cdc42 interacting protein 4, Biochim. Biophys. Acta 1862 (2016) 1172–1178.
[20] A.K. Howe, Regulation of actin-based cell migration by cAMP/PKA, Biochim. Biophys. Acta 1692 (2004) 159–174.
[21] P.H. Schmidt, D.T. Dransfield, J.O. Claudio, R.G. Hawley, K.W. Trotter, S.L. Milgram, et al., AKAP350, a multiply spliced protein kinase A-anchoring protein associated with centrosomes, J. Biol. Chem. 274 (1999) 3055–3066.
[22] H. Dinkel, C. Chica, A. Via, C.M. Gould, L.J. Jensen, T.J. Gibson, et al., Phospho.ELM: a database of phosphorylation sites- update, Nucleic Acids Res. 39 (2011) D261–D267.
[23] Y. Xue, A. Li, L. Wang, H. Feng, X. Yao, PPSP: prediction of PK-specific phosphorylation site with Bayesian decision theory, BMC Bioinf. 7 (2006) 163.
[24] V.V. Artym, Y. Zhang, F. Seillier-Moiseiwitsch, K.M. Yamada, S.C. Mueller, Dynamic interactions of cortactin and membrane type 1 matrix metalloproteinase at invadopodia: defining the stages of invadopodia formation and function, Cancer Res. 66 (2006) 3034–3043.
[25] A.K. Kenworthy, M. Edidin, Distribution of a glycosylphosphatidylinositol -anchored protein at the apical surface of MDCK cells examined at a resolution of < 100 A using imaging fluorescence resonance energy transfer, J. Cell Biol. 142 (1998) 69–84.
[26] S. Etienne-Manneville, Microtubules in cell migration, Annu. Rev. Cell Dev. Biol. 29 (2013) 471–499.
[27] A.C. Ferretti, F. Hidalgo, F. Tonucci, E. Almada, A. Pariani, M.C. Larocca, C. Favre, Metformin and glucose starvation decrease the migratory ability of hepatocellular carcinoma cells: targeting AMPK activation to control migration, Sci. Rep. 9 (2019) 2815.
[28] M. Fernandez-Gallardo, R. González-Ramírez, A. Sandoval, R. Felix, E. Monjaraz, Adenosine stimulate proliferation and migration in triple negative breast cancer cells, PLoS One 11 (2016) e0167445.
[29] A. Caretta, C. Mucignat-Caretta, Protein kinase a in cancer, Cancers 3 (2011) 913–926.
[30] W. Wong, J.D. Scott, AKAP signalling complexes: focal points in space and time, Nat. Rev. Mol. Cell Biol. 5 (2004) 959–970.
[31] F.D. Smith, J.L. Esseltine, P.J. Nygren, D. Veesler, D.P. Byrne, M. Vonderach, et al., Local protein kinase A action proceeds through intact holoenzymes, Science 356 (2017) 1288–1293.
[32] A.G. Beristain, S.D. Molyneux, P.A. Joshi, N.C. Pomroy, M.A. Di Grappa, M.C. Chang, et al., PKA signaling drives mammary tumorigenesis through Src, Oncogene 34 (2015) 1160–1173.
[33] Y. Wang, Y. Chen, M. Chen, W. Xu, AKAPs competing peptide HT31 disrupts the inhibitory effect of PKA on RhoA activity, Oncol. Rep. 16 (2006) 755–761.
[34] A. Leibfried, R. Fricke, M.J. Morgan, S. Bogdan, Y. Bellaiche, Drosophila Cip4 and WASp define a branch of the Cdc42-Par6-aPKC pathway regulating E-cadherin endocytosis, Curr. Biol. 18 (2008) 1639–1648.
[35] H. Miki, T. Takenawa, Regulation of actin dynamics by WASP family proteins, J. Biochem. (Tokyo) 134 (2003) 309–313.
[36] M. Lorenz, H. Yamaguchi, Y. Wang, R.H. Singer, J. Condeelis, Imaging sites of N-WASP activity in lamellipodia and invadopodia of carcinoma cells, Curr. Biol. 14 (2004) 697.
[37] J.R. Watson, H.M. Fox, D. Nietlispach, J.L. Gallop, D. Owen, H.R. Mott, Investigation of the Interaction between Cdc42 and its Effector TOCA1: handover of CDC42 to the actin regulator N-WASP is facilitated by differential binding affinities, J. Biol. Chem. 291 (2016) 13875–13890.
[38] A. Shimada, H. Niwa, K. Tsujita, S. Suetsugu, K. Nitta, K. Hanawa-Suetsugu, et al., Curved EFC/F-BAR-domain dimers are joined end to end into a filament for membrane invagination in endocytosis, Cell 129 (2007) 761–772.
[39] W. Saengsawang, K.L. Taylor, D.C. Lumbard, K. Mitok, A. Price, L. Pietila, et al., CIP4 coordinates with phospholipids and actin-associated proteins to localize to the protruding edge and produce actin ribs and veils, J. Cell Sci. 126 (2013) 2411–2423.